Scientific goals for the observation of Venus by VIRTIS on ESA/Venus express mission

P. Drossart[a,*], G. Piccioni[b], A. Adriani[c], F. Angrilli[d], G. Arnold[e], K.H. Baines[f], G. Bellucci[b], J. Benkhoff[e], B. Bézard[a], J.-P. Bibring[g], A. Blanco[h], M.I. Blecka[i], R.W. Carlson[f], A. Coradini[c], A. Di Lellis[b], T. Encrenaz[a], S. Erard[a], S. Fonti[h], V. Formisano[c], T. Fouchet[a], R. Garcia[j], R. Haus[e], J. Helbert[e], N.I. Ignatiev[k], P.G.J. Irwin[l], Y. Langevin[g], S. Lebonnois[m], M.A. Lopez-Valverde[n], D. Luz[a,o], L. Marinangeli[p], V. Orofino[h], A.V. Rodin[k], M.C. Roos-Serote[o], B. Saggin[q], A. Sanchez-Lavega[r], D.M. Stam[s], F.W. Taylor[l], D. Titov[t], G. Visconti[p], M. Zambelli[b], R. Hueso[r], C.C.C. Tsang[l], C.F. Wilson[l], T.Z. Afanasenko[k]

[a]*LESIA, Observatoire de Paris (CNRS-UMR 8109), 5 place Jules Janssen, 92195 Meudon, France*
[b]*INAF-IASF, Via del Fosso del Cavaliere, 100 00133 Rome, Italy*
[c]*INAF-IFSI, Via del Fosso del Cavaliere, 100 00133 Rome, Italy*
[d]*CISAS, Via Venezia, 15-35131 Padova, Italy*
[e]*Deutsche Zentrum für Luft und Raumfahrt, Rutherfordstraße 2, 12489 Berlin, Germany*
[f]*Jet Propulsion Laboratory, California Institute of Technology, M/S 183-601, 4800 Oak Grove Drive, Pasadena, CA 91109, USA*
[g]*IAS, Batiment 121, 91405 Orsay Campus, France*
[h]*Università di Lecce, CP 193, Via Arnesano, Lecce, Italy*
[i]*Space Research Centre, ul. Bartycka 18A, 00-716 Warszawa, Poland*
[j]*IPGP, Université Paris 7, UMR7154 4, ave de Neptune, 94107 St. Maur, France*
[k]*Space Research Institute (IKI), Profsoyuznaya 84/32, Moscow, Russian Federation*
[l]*University of Oxford, Parks Road, Oxford OX1 3PU, England, UK*
[m]*Laboratoire de Meteorologie Dynamique, Jussieu, P.O. Box 99, Paris cedex 05, France*
[n]*Instituto de Astrofisica de Andalucia (I.A.A.), Apdo. 3004, 18080 Granada, Spain*
[o]*CAAUL/Observatorio Astronomica de Lisboa, Tapada da Ajuda, 1349-018 Lisboa, Portugal*
[p]*Universita' d'Annunzio, Viale Pindaro 42, 65127 Pescara, Italy*
[q]*Politecnico di Milano, Via Marco D'Oggiono 18/A, 23900 Lecco, Italy*
[r]*Escuela Superior Ingeniería, Universidad País Vasco, Alameda Urquijo, s/n 48013 Bilbao, Spain*
[s]*Astronomical Institute "Anton Pannekoek" Kruislaan 403, 1098 SJ Amsterdam, The Netherlands*
[t]*Max Planck Institute for Solar System Studies, Max-Planck-Str. 2, 37191 Katlenburg-Lindau, Germany*

Abstract

The Visible and Infrared Thermal Imaging Spectrometer (VIRTIS) on board the ESA/Venus Express mission has technical specifications well suited for many science objectives of Venus exploration. VIRTIS will both comprehensively explore a plethora of atmospheric properties and processes and map optical properties of the surface through its three channels, VIRTIS-M-vis (imaging spectrometer in the 0.3–1 μm range), VIRTIS-M-IR (imaging spectrometer in the 1–5 μm range) and VIRTIS-H (aperture high-resolution spectrometer in the 2–5 μm range). The atmospheric composition below the clouds will be repeatedly measured in the night side infrared windows over a wide range of latitudes and longitudes, thereby providing information on Venus's chemical cycles. In particular, CO, H_2O, OCS and SO_2 can be studied. The cloud structure will be repeatedly mapped from the brightness contrasts in the near-infrared night side windows, providing new insights into Venusian meteorology. The global circulation and local dynamics of Venus will be extensively studied from infrared and visible spectral images. The thermal structure above the clouds will be retrieved in the night

*Corresponding author. Tel.: +33 1 45 07 76 64; fax: +33 1 45 07 71 10.
E-mail addresses:* pierre.drossart@obspm.fr (P. Drossart), giuseppe.piccioni@iasf-roma.inaf.it (G. Piccioni).

side using the 4.3 μm fundamental band of CO_2. The surface of Venus is detectable in the short-wave infrared windows on the night side at 1.01, 1.10 and 1.18 μm, providing constraints on surface properties and the extent of active volcanism. Many more tentative studies are also possible, such as lightning detection, the composition of volcanic emissions, and mesospheric wave propagation.

1. Introduction

The Visible and Infrared Thermal Imaging Spectrometer (VIRTIS) on Venus Express is an imaging spectrometer directly inherited from that on the Rosetta mission (Coradini et al., 1999). It builds on the legacy of previous instruments which combine imaging and spectroscopy in the near infrared, like Galileo/NIMS (NIMS—near infrared mapping spectrometer) (Carlson et al., 1992), Cassini/ VIMS (VIMS—visible-infrared mapping spectrometer) (Brown et al., 2004) and Mars Express/OMEGA (Bibring et al., 2005). The first version of the VIRTIS instrument is currently en route to comet 67P/Churyumov–Gerasimenko, as part of the scientific payload of the Rosetta mission.

Observations of Venus with near infrared spectroscopy and spectral imaging have been performed since the 1980s from both the ground and from the fast Venus flybys of the Galileo and Cassini spacecraft, in February 1990 and December 2000, respectively. Such pioneering observations demonstrated the unique ability of the near-infrared to enable three-dimensional studies of the atmosphere, especially by providing a novel means to penetrate the planet's thick cloud deck to access the deep atmosphere and surface. The VIRTIS experiment on Venus Express expands on these experiences, capitalizing on both (1) the evolution of technology (in particular the use of two-dimensional infrared detector arrays) and (2) the long-term temporal and global spatial coverage provided by a planetary orbiter. Venus Express orbital operations are scheduled for a nominal mission of 500 days, with a possible extended mission of another 500 days or more (Svedhem et al., 2007). This relatively long duration mission will allow phenomena on Venus to be studied over time scales ranging from minutes to several years.

Since the discovery of the night side infrared windows between 1.5 and 2.5 μm by Allen and Crawford (1984), ground-based observations have periodically provided new details of the deep atmospheric structure of Venus. A review of the large amount of work obtained by spectroscopy and imaging spectroscopy from the ground is given by Taylor et al. (1997).

Unfortunately, ground-based observations offer only very limited temporal and spatial coverage of Venus, since they depend upon a favourable geometric alignment of Venus and Earth with night side observations limited to the period from quadrature to inferior conjunction. During this time, the dark side of Venus covers at most two-thirds of the disk as viewed from Earth. Due to the proximity of the planet to the sun in the sky near conjunction, observations from any one observatory are typically limited to just an hour after sunset or before sunrise, limiting temporal studies. Furthermore, the commensurability of Venus's rotation with Earth's orbit means that Venus always presents the same hemisphere to Earth during conjunction. Thus, ground-based coverage is limited to a specific area covering less than a third of the globe. The slow retrograde rotation of Venus exacerbates the situation, limiting the range of sub-Earth Venus longitudes to just a few degrees during this 2-month observing period.

The first unique near infrared studies from space were provided by the Galileo Venus flyby in 1990, from which the NIMS obtained spectacular views of the deep cloud structure, and detected surface features in the near infrared window at 1.18 μm. Despite its short duration, this flyby provided new results on the cloud structure, the atmospheric composition, and even the dynamics (Carlson and Taylor, 1993).

A second encounter with Venus was provided by Cassini in late 2000. Due to operational constraints, VIMS observations were limited to the visible channel only, but nevertheless provided a detection of the surface of Venus in the very near infrared windows at 1.01 and 1.10 μm (Baines et al., 2000).

VIRTIS on Venus Express will therefore benefit from the considerable experience accumulated by ground-based observers and precursor space experiments on Venus, and will have more in-depth capabilities thanks to a long duration orbital mission, a higher spatial resolution due to the proximity of the spacecraft to the planet, and a polar orbit allowing direct viewing of the polar regions.

This paper is organized as follows: after a description of the VIRTIS instrument (Section 1) and calibration, archiving and navigation processing (Section 2), the science objectives obtained through radiative transfer studies are described in Section 3 and surface science objectives in Section 4. Dynamics objectives are described in Section 5, and finally some more tentative observational goals are listed in Section 6.

2. VIRTIS description

A full technical description of VIRTIS is given in Piccioni et al. (2006), with only a summary here. The Visible and Infrared Thermal Imaging Spectrometer is a dual instrument with separate telescopes supplying two channels: (1) VIRTIS-M, a mapping spectrometer working in the visible (VIRTIS-M-vis from 0.3 to 1 μm) and in the

infrared (VIRTIS-M-IR from 1 to 5 μm) and (2) VIRTIS-H, a high-resolution spectrometer with a spectral range in the infrared 2–5 μm. It was proposed for the Rosetta mission (Coradini et al., 1999), to study the properties of a cometary surface (the main objective of VIRTIS-M), and of the coma (the main objective of VIRTIS-H). Thanks to the high versatility of the observing modes—in particular the flexibility to choose different repetition times and integration times—the specifications of VIRTIS were also found to be suitable for the study of the atmosphere of Venus. When the Venus Express mission was proposed to ESA, it was therefore a natural element of the model payload, particularly as it was possible to re-use the Rosetta flight spare model.

The main characteristics of VIRTIS are given in Table 1. The instantaneous field of view (IFOV) of VIRTIS-M over the whole slit is 0.25×64 mrad, corresponding to about one-third of the diameter of Venus at apocenter 60,000 km from the planet. VIRTIS-H has a larger IFOV of 0.5×1.5 mrad. The total field of view is 64 mrad after taking account of scanning by the secondary mirror of the telescope, which has 256 positions. Therefore, VIRTIS global observations need a 3×3 mosaicing procedure at apocenter (Case 3 of science operations—see article by Titov et al., 2006). Alternatively, VIRTIS can be limited to a regional survey over a selected part of the disk of Venus (Case 2). At pericenter (Case 1), the spacecraft is only about 350 km above the cloud tops, and the field of view on Venus is very small. Imaging with VIRTIS then becomes problematic, since the dwell time is shorter than the integration time. Periapsis mapping will therefore be devoted to statistical sampling over the accessible area, with spectroscopy measurements made over a large range of latitudes. Limb observations can also be performed near periapsis with Venus Express in 3-axis stabilized mode and VIRTIS-M in slit mode (no 2D scan).

2.1. Calibration

Due to the thermal environment at Venus, the VIRTIS calibration process on Venus Express has some unique features compared to that used by the Rosetta mission. In particular, the cold box of the instrument can reach temperatures between 150 and 160 K, while on Rosetta the nominal temperature is 135 K. The thermal emission of the Venus Express instrument is consequently much stronger than on Rosetta, and dark subtraction is an important step in raw data calibration. Spectral and radiometric calibration is performed using pre-launch measurements, as well as data retrieved in space, by the internal calibration procedure. The cold box temperatures are expected to vary during the orbit around Venus, due to the relative configuration of the spacecraft, Venus and the Sun, inducing variations in the dark frames in the infrared channels (VIRTIS-M-IR and VIRTIS-H), which have to be corrected for proper science analysis.

2.2. Data handling and archiving

The routine science operations of the VIRTIS instrument on board are managed through the Venus Science Operation Center-PI interface. The instrument timelines along the proper spacecraft commanding files are submitted to the ESA server in a monthly base for the Medium Term Plan and a weekly period for the short-term plan. From the IASF-Rome site which collects also the VIRTIS-H specific timelines from LESIA-Paris. Once the data are collected, the telemetry from the spacecraft is first handled and preprocessed by ESA, including checking of data packets and the addition of a header containing a translation in UTC of the corresponding on-board times. The data are then made available to the PI teams in Rome and Paris through requests sent from IASF-Rome to the Venus Express data disposition system at ESOC. The prime archive contains both the Telecommand (TC) files and the received telemetry packets (TM).

VIRTIS TM packets are then processed by the ground segment of the instrument (EGSE), the functions of which include:

- Checking data integrity and instrument functioning.
- Reordering of TM packets according to acquisition time.

Table 1
Main characteristics of the VIRTIS instrument

Parameter	VIRTIS-M		VIRTIS-H
	Visible	Infrared	Infrared
Spectral range (μm)	0.27–1.1	1.05–5.19	1.84–4.99
Spectral sampling (nm)	1.9	9.8	0.6
FOV (mrad^2)	64×64		0.58×1.75 per 3 pixels
Pupil diameter (mm)	47.5		32
$F\sharp$	5.6	3.2	2.04
Etendue (m$^2 \times$ sr)	3.6×10^{-11}	7.5×10^{-11}	0.8×10^{-9}
Slit dimension	38 μm $\times$ 9.53 mm		29×89 μm
Detector format (p $\times$)	512×1024	270×438	270×438
Pixel pitch (μm)	19	38	38
Saturation charge (Me)	>0.4	>2	>2

- Data decompression.
- Quick look of both data and housekeeping/event parameters.
- Writing of Planetary Data System (PDS) raw data files.

The use of the PDS format ensures that the VIRTIS files will be readable by many kind of software (ENVI, ISIS, etc.); and compliant to the Planetary Science Archive (PSA) format of ESA, which is a specific version of PDS, for long-term archiving.

Data from the three focal plane arrays (FPAs) are stored separately in decompressed format; each file corresponds to a sub-session, with one channel of VIRTIS (VIRTIS-M-vis, VIRTIS-M-IR and VIRTIS-H), in a unique observation mode. Data are organized as PDS objects known as Cubes. Housekeeping parameters used by the data calibration procedure are stored in the sideplane of each cube and a PDS label (in ASCII format) is attached on top of the file.

Data storage in the PDS files is determined by the data production mode of the instrument:

- *For VIRTIS-M*, data from the Visible and the IR FPA are stored in different files, so as to simplify data handling. For each FPA, science data and dark frames are stored in the same file, interleaved in the cube core in order of acquisition.

  The format structure for in flight calibrations data and all science data is similar but the cube size may be different depending on the specific operation mode. The most demanding mode in terms of data volume is called "All pix full win" which corresponds to a format of 256×256 spatial pixels by 432 spectral wavelengths. To cope with different resources availability along the mission, a binning may be applied for the spatial direction (factor 4) or the spectral direction (factor 3). In addition, three different lossy compressions may be used instead of the default lossless compression in the case of a very limited data rate period.

  All the modes may be operated without scanning mechanism (fixed mirror, push-broom mode) or with scanning mechanism depending on the observation geometry conditions.
- *For VIRTIS-H*, data are transferred according to one of three possible transfer modes: "image" (432×256 pixels), "spectrum" (sequence of 3456 measurements), and "64-spectra slice" (groups of 64 spectra compressed together). The data transferred through different modes cannot be stored together in a cube object, because of their different dimensions. The operating modes are combinations of these three transfer modes, and therefore a specific data storage scheme is defined for each. These include:
  - *Nominal mode*: Spectra are reconstructed on board from the FPA images. Measurements are grouped by sets of 64 spectra compressed together, and transferred as "64-spectra slice"; they are interleaved with dark measurements transferred as "spectrum". Two files are written in parallel: a first cube containing the measured spectra grouped in sets of 64 ($3456 \times 64 \times$ sequence length); and a second cube containing the dark spectra ($3456 \times 1 \times$ number of dark spectra). The number of dark measurements associated with one "spectral slice" depends on operational parameters. The two files are synchronized using the SCET (on board acquisition time) stored in the sideplanes.
  - *"Backup" mode (or "full frame mode")*: No spectrum reconstruction is performed; measurements and interleaved dark frames are transferred as full FPA images. Only one file is written: a cube containing the measured image frames and dark frames ($432 \times 256 \times$ number of images acquired).
  - *Calibration mode*: A group of seven images and a group of two spectra are acquired in sequence. Two short files are written: a first cube containing the seven images of the detector ($432 \times 256 \times 7$); another cube containing the spectrum and its associated dark frame ($3456 \times 1 \times 2$).

In all cases, each frame of the cube core is associated with a frame in the sideplane that contains the housekeeping parameters acquired simultaneously. The VIRTIS sideplane structure is unusual, because the ISIS/PDS cube definition is poorly adapted to modern instruments. Since, the downloading rate of housekeeping parameters is completely independent of the data rate, and because the dimensions of a frame can be rather large, storing housekeeping parameters the usual way would result in a huge waste of space, with files containing more zeroes than data in some situations. Instead, housekeeping and ancillary information is packed as much as possible. It is grouped in fixed sequences (82 parameters for M, 72 for H) which are stored end to end in the sideplane rows, and extra rows are added whenever needed.

Finally, the labels use a subset of PDS keywords and syntactic rules according to PSA requirements; some non-standard keywords are defined at mission level and are introduced by a namespace.

Navigation information is received from ESA in the form of Spice kernels. This information is used to compute projection of the data on Venus, viewing angles, local time, surface and elevation, etc., on a pixel basis, using the Spice library. The geometry information is stored in PDS cubes with one-to-one correspondence to data cubes. Data sets are projected along the line of sight on two reference layers, representing the surface and the upper cloud layer. The surface layer is the IAU 2000 ellipsoid (Seidelmann et al., 2002), while the reference cloud layer is a chosen to be a shell located at 60 km altitude. Although, most photons actually originate from the upper atmosphere and the weak signal from the surface is expected to be strongly bended and blurred by scattering and refraction, this system allows the investigators to interpolate any parameter at

intermediate altitudes easily if needed. Surface elevation is provided both in the surface footprint, and below the intercept with the cloud layer; the surface elevation model used is the Magellan GTDR (Ford, 1991). For limb observations, the impact parameter is provided instead. Other quantities such as local time at footprint, sub-spacecraft coordinates, sub-solar point, season, etc. are also included in the geometry files.

All of the information contained in the data labels and sideplanes is ingested into a database maintained at Meudon. A description of the operational and observational conditions is also stored in the database, in particular from the Science Activity Plan. This allows monitoring of the instrument and data during operations, and generation of PDS catalogues and index files at the time of delivery to the PSA. The archive also preserves raw data files, geometry files, and basic software to access and calibrate the data, plus catalogues, indices, and calibration files.

This information constitutes the Experimental Data Record (EDR) or level 2 data set. Calibrated (level 3) data consist of data in physical units (in radiance) plus description of viewing configuration (viewing angles, location, local time and season). Spectral and spatial

redundancies are preserved in level 3 data, with estimates of spectral and radiance accuracy. Calibration as I/F ratio can be performed using as scaled solar spectrum derived from Kurucz (1998), and convolved with VIRTIS spectral responses (Fig. 1).

2.3. Navigation and processing of VIRTIS-M cube images

The navigation and processing of VIRTIS-M cube images starts from the PDS data and geometry cubes described in the previous section. In the VIRTIS experiment a further difficulty is image restoration, since the VIRTIS-M cube images are obtained at different spatial resolutions and at different latitudes on the planet depending on the orbit position (see science cases description by Titov et al., 2006). Due to the orbital velocity of Venus Express, VIRTIS image reconstruction is possible only in cases 2 and 3, when the spacecraft is at distances larger than $\sim$10,000 km. Therefore, cloud tracking and dynamic studies can be performed accurately on the whole Southern Hemisphere, but very limited information will be obtained of the northern hemisphere in imaging mode.

Since the spectral range of the VIRTIS-M experiment is fairly wide, spectral image cubes contain simultaneous
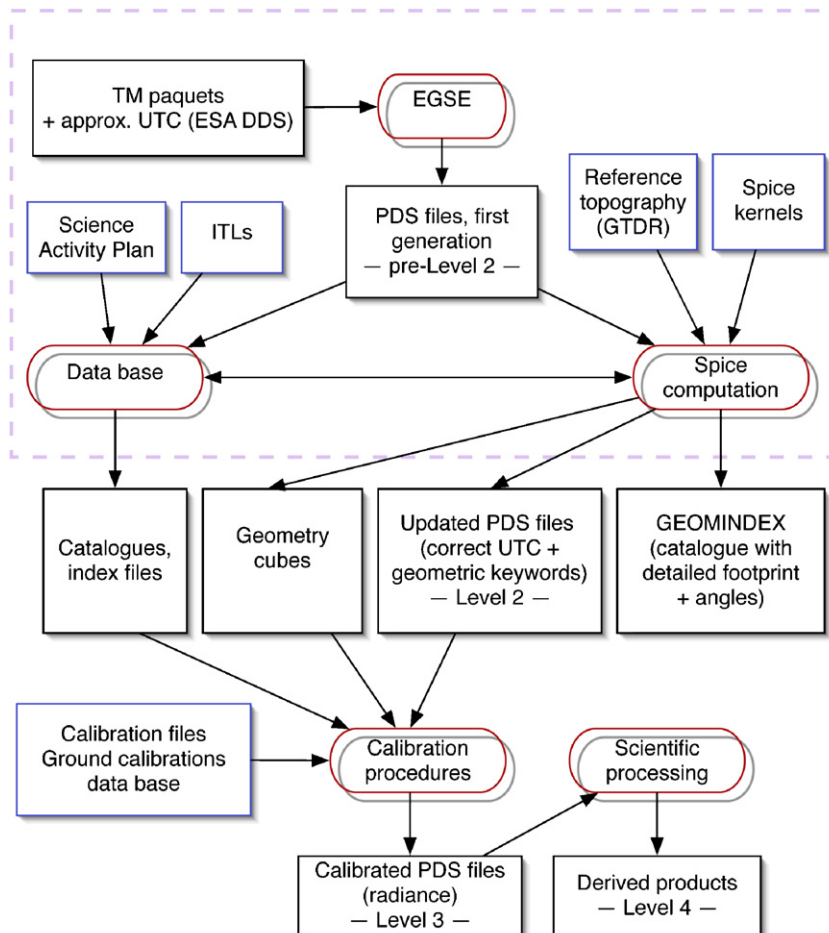

Fig. 1. Chart of VIRTIS pipe-line data processing from TM data to cubes.

information on cloud features at different altitude levels (see Part 3). A number of image processing techniques can be used to improve the ability to identify cloud features and perform wind tracking, or simply improve the signal/noise ratio and the local contrast in order to increase the detection and identification of the clouds tracers. One useful method to analyse near-wavelength images is Principal Component Analysis (PCA) traditionally used to increase local contrasts and image quality by combining information of different colour channels into a well contrasted monochromatic image (Irwin and Dyudina, 2002). The ability to project images from the spherical geometry of the planet to cylindrical projections proved to be very useful in the cloud tracking analysis of the Galileo Orbiter observations of Venus (Toigo et al., 1994).

These software features have been implemented in a graphical user interface program running under IDL called PLIA (Planetary Laboratory and Image Analysis). PLIA is used to navigate the cube images, extract information at different wavelengths, compose sets of them for PCA, perform limb darkening corrections, track clouds and measure winds, compose images of different wavelengths, obtain photometrical cuts of the images for cloud structure analysis, and perform geometrical projections such as polar or cylindrical mapping of the planet. The software allows several image manipulations to improve feature identification. Those currently implemented are: unsharp mask, Laplacian filters, image stacking of different cubes and/or same cube nearby wavelengths. Additionally, we have found that specific Butterworth filters in inverse Fourier space (González and Woods, 2002) are a very powerful tool to increase the visual contrast of the upper clouds at the characteristic scales of cloud variability. To test PLIA we used Galileo single wavelength observations of Venus dating from 1990 (Belton et al., 1991). Fig. 2 shows some of the preliminary results: (a) image navigation, (b) rectilinear projection, (c) zonal reflectivity scans at different latitudes and (d) cloud tracking and zonal wind measurements.

3. Radiative transfer modelling

3.1. Retrievals of atmospheric composition

3.1.1. Night side observations

An important goal of VIRTIS is mapping and monitoring the composition of Venus' deep atmosphere below the clouds using spectral imaging in the night side windows between 1.0 and 2.5 μm. Information on the CO, H_2O, OCS and SO_2 abundances in the range 26–45 km is available from the 2.3-μm window while the 1.7-μm narrower window, provides information on the H_2O and HCl abundances in the 15–30 km altitude region (Taylor et al., 1997). The most transparent windows at 1.0, 1.10 and 1.18 μm allow probing of the H_2O profile in the lowest scale height of the atmosphere (0–15 km) (e.g., de Bergh et al., 1995). Besides H_2O, vertically resolved information will be obtained for CO and OCS from the shape of their

absorption bands in the 2.3-μm window, as first shown by Pollack et al. (1993). In addition, the D/H ratio will be determined from the simultaneous analysis of the HDO and H_2O lines in the 2.3-μm window, preferentially in the VIRTIS-H mode for higher spectral resolution.

Horizontal or time variations in the sub-cloud composition could arise from the general atmospheric circulation, local meteorology, or active volcanism if present. Recently, Marcq et al. (2005, 2006) derived latitudinal variations in the CO and OCS abundances using ground-based observations of the 2.3-μm window at a spectral resolution similar to VIRTIS-M. The CO abundance was found to increase by about 15% between the equator and higher latitudes (40°N or S) while the OCS abundance exhibits anticorrelated variations. Such variations can be interpreted as due to the large-scale circulation with upwelling in the equatorial region and downwelling at high latitudes. In this same study, no variations within 10% were observed for H_2O (in the 30–40 km height range). In contrast, Bell et al. (1991) once observed a strong localized enhancement in the H_2O absorption over a bright region on the night side. The derived factor of 5 increase in the abundance was attributed to subsidence and evaporation of H_2SO_4 droplets. VIRTIS will clearly improve over such ground-based studies by providing a higher spatial resolution and a much better view of high latitudes. In addition, VIRTIS night side observations will not suffer from contamination by scattered light from the dayside and telluric absorption which have been shown to be the limiting factors of the precision with which horizontal variations can be mapped from Earth (Marcq et al., 2005, 2006). A precision of 5% or better, at least for the major absorbers (CO, OCS, H_2O), should be achieved by VIRTIS-M, being ultimately limited by precision in the flat fielding and possibly by the noise level. Finally, VIRTIS will be a sensitive tool to search for possible active volcanism. Besides surface temperature enhancement observable in the 1.0–1.2 μm windows, volcanic activity could result in local enhancements of sulphur gases (HDO, OCS, SO_2) or emission of still undetected compounds (e.g., CH_4). These gases will be monitored with a high precision and good spatial resolution by VIRTIS-M.

It is important to note that the uncertainty in the absolute abundances of the various absorbers may eventually depend on the accuracy of the radiative transfer modelling used to derive such quantities. The main source of opacity in the near-infrared windows derives from the far wings of the strong CO_2 bands at the edges of the windows, pressure-induced CO_2 bands, and weak allowed CO_2 bands. The latter are modelled using Wattson's high-temperature database as described in Pollack et al. (1993). This allows a reasonable reproduction of the CO_2 bands present in the windows although some improvement would be desirable to remove a few discrepancies. The major issue however is the continuum-like opacity resulting from CO_2 far wings and pressure-induced bands (Tonkov et al., 1996). This limits the depth probed by the near-infrared
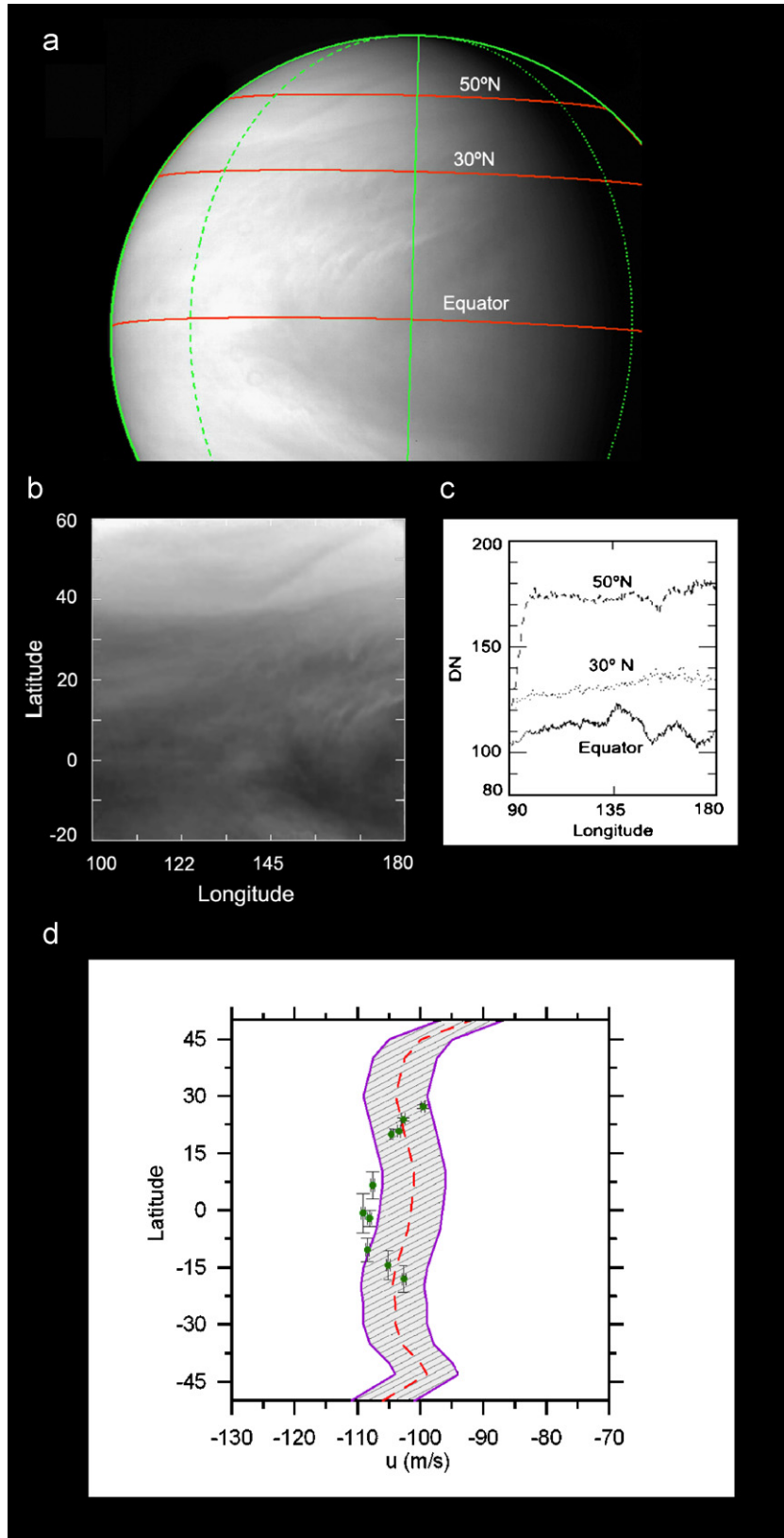
Fig. 2. Preliminary tests of PLIA software using Galileo SSI UV image frame 18530200 acquired on 13 February 1990: (a) contrast stretched original image, with three latitudinal parallels at 0, 30 and 50°N marked; (b) high-resolution rectilinear projection of the original image (resolution 0.25°/pix); (c) reflectivity scans corrected for limb-darkening effects at the previous three latitudes; (d) zonal wind velocity profile. Dots are wind measurements performed with PLIA in two Galileo images separated by 4 days. The central dashed line shows the wind profile retrieved over a different Galileo data set by Toigo et al. (1994). The shaded region shows the estimated uncertainty over these measurements related to the 1-h time interval used by the Galileo Imaging Team. Our measurements over a full atmospheric rotation (4 days) are much more accurate.

windows and uncertainties in this absorption translates into an uncertainty in the retrieved abundances of other gases.

Although numerous studies have been devoted to the issue of line shapes in the last decades, including state-of-the-art theoretical studies, including line-mixing effects (e.g., Ma and Tipping, 1991; Filippov and Tonkov, 1998), they do not really offer a model suitable for practical calculations. In most cases, simulations of Venus' atmospheric spectra made use of empirical or semi-empirical form factors based on piecewise exponential approximations fitting laboratory data at high pressure and temperature (e.g., Burch and Gryvnak, 1971). In contrast with the conventional Lorentz line shape, such sub-Lorentzian models are capable of reproducing observations with a good precision (e.g., Bézard et al., 1990; Taylor et al., 1997; Bullock and Grinspoon, 2001). However, they do not describe the dependence of the form factor with temperature and do not treat explicitly the line mixing. Thus, the accuracy of such calculations may be improved by using more detailed, physically grounded, line shape models. A possibility is using the theory of far wing developed by Tvorogov and Rodimova (1995), which treats the intermolecular interaction in terms of quantum mechanics, while formulating the kinetic problem in terms of classical statistical physics. Despite the difficulties in determining the needed parameters for numerous CO_2 bands, implementation of such or similar models is a necessary step toward deeper insight into spectroscopy of the exceptionally dense Venus atmosphere.

A detailed description of the far-wing model and its implications for the radiative transfer in the Venus atmosphere is presented by Afanasenko and Rodin (2005). In Fig. 3, we show an example of spectral absorption of CO_2 in the vicinity of the 4.3 μm band edge, calculated by means of the line mixing model (solid curve), adapted from
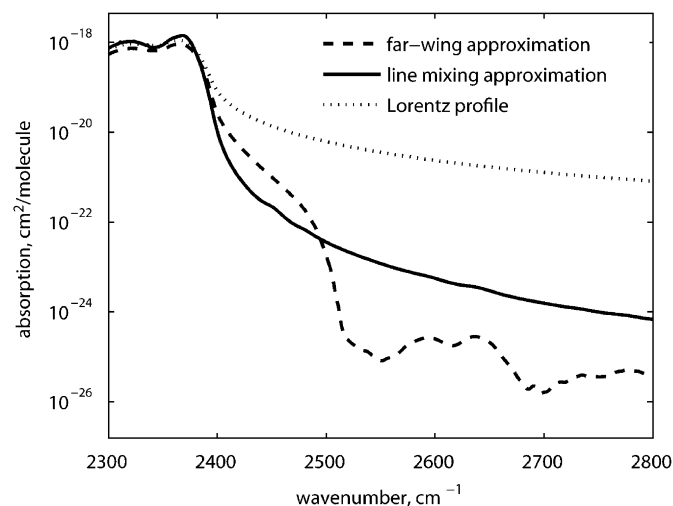

Fig. 3. Spectral absorption of CO_2 near the surface of Venus calculated for different models. Solid curve: line mixing model in strong collision approximation; dashed curve: far wing approximation; dotted curve; pure Lorentz profile.

Filippov and Tonkov (1996) and the far wing approximation (dashed curve), derived from a model adapted from Tvorogov and Rodimova (1995), for conditions corresponding to the lower Venus atmosphere.

An unphysical spectrum that would result from application of the Lorentzian form-factor to the whole range is shown by the dotted curve for comparison. It is seen that both models yield comparable absorption spectra behind the band edge, although they differ by an order of magnitude at some wavelengths. In the farthest region, the exponential model decays faster, but for practical calculations these regions may be dominated by absorption of minor constituents. Since the parameters of the exponential model has been fitted without taking into account the line mixing effect, both models approximate essentially the same experimental result. The implication of both assumptions–the mixing effect in the line core and the exponential far wings–is a realistic method for the simulation of radiative transfer on Venus. However, this would require independent fitting of parameters incorporated in the far wing theory. Despite the remarkable difficulties in determining these parameters for numerous CO_2 bands, the implementation of these or similar models is a necessary step toward deeper insight into the spectroscopy of the exceptionally dense Venus atmosphere.

Longward of 3 μm, the thermal emission on the night side originates from the cloud tops. By observing the (1–0) CO band with VIRTIS-H, both at various emission angles and in a limb-viewing geometry, it will be possible to retrieve the CO vertical profile from about 70 to 84 km. Horizontal variations of this compound will provide important constraints on the photochemistry of CO_2 and on the transport mechanisms at and above the cloud tops.

3.1.2. Dayside observations

Besides CO_2, molecular bands of CO and H_2O can be detected on the dayside in the VIRTIS spectral range. CO was detected from the ground by high-resolution spectroscopy (Connes et al., 1968). Dayside observations can measure molecular absorptions above the cloud top; CO_2 bands can be used to retrieve the cloud deck altitude variation. Weak CO_2 bands (e.g., 2.5 μm) will be chosen to get comparable absorptions between CO_2 and the minor constituents, and mostly eliminate the uncertainty due to variations in the cloud tops. These measurements are nevertheless challenging, as the abundance of CO and H_2O above the clouds is very small. Using spectra with large viewing angle, or at the limb, should facilitate these detections.

3.2. Temperature field and cloud structure

Within the VIRTIS thermal spectral range (3–5 μm) it is possible to study the structure of the atmosphere and the clouds from the ~65-km altitude cloud deck up to about 90 km. In this wavelength range, thermal emission from the clouds forms the continuum with an average brightness

temperature of 235 K. Two bands of carbon dioxide are present: the very strong ν_3 band between 4 and 4.5 μm and the weaker overtone $\nu_1 + \nu_2$ band centred at 4.85 μm. In addition the (1–0) band of CO occurs around 4.7 μm. The continuum wavelengths contain information about the cloud top temperature, the cloud particle scale height and the scattering properties of the particles.

The most recent data set covering this spectral range was collected by the Galileo NIMS, at a spectral resolution of 0.025 μm during the Galileo Venus flyby in February 1990. Observations were made on both the night and the dayside of Venus. However, on the dayside the solar reflected light contributed significantly to the radiation and non-LTE effects dominate the carbon dioxide ν_3 band centre.

Roos et al. (1993) and Roos-Serote et al. (1995) used the night side NIMS thermal data to study both the cloud and thermal structure of the atmosphere between 60 and 90 km of altitude. Roos et al. (1993) used limb-darkening measurements in the longitudinal direction at six continuum wavelengths and found that the zonally averaged cloud particle scale height is essentially constant in the latitude region between $-25°$ and $+30°$. They first applied a simple model with no scattering to describe the limb-darkening effect. This resulted in an average value of 4.1 ± 0.6 km for the cloud particle scale height (zonal average) between $-25°$ and $+30°$. A more elaborated model including Mie scattering was then applied to the data in one wavelength band, leading to a value of 5.2 ± 0.8 km. Both values are consistent within error bars and agree with results from the analysis of previous data sets such as Pioneer Venus and ground-based observations.

With the VIRTIS data it will be possible to do a much more extended study of the cloud structure as a function of latitude. It will also be possible to get a better handle on the cloud particle shapes and scattering phase function from dayside studies (feature tracking), and consequently to model the night side limb-darkening effect more accurately.

Roos et al. (1993) found that the cloud temperature at unit optical depth as derived from the six NIMS thermal wavelength bands shows an absorption feature with a minimum at 4 μm. Earlier studies (Pollack et al., 1978) showed that the reflectivity in the 2.5–4 μm range is compatible with a cloud particle composition containing 84% of sulphuric acid. Roos et al. (1993) were unable to identify a possible absorber to explain this feature. With VIRTIS, it will be possible to study the cloud reflectivity in great detail on the dayside of the planet and possibly identify this spectral feature.

From the ν_3 CO_2 absorption band, Roos-Serote et al. (1995) inferred the temperature profile as a function of latitude. The NIMS data set contains 12 spectra at 3 am Venus local time ranging from $-69°$ to $+75°$. From the centre to the edges of the absorption band, levels between 90 and 75 km altitude are probed, with a vertical resolution on the order of 10 km (FWHM of the weighting functions).

From the 12 temperature profiles, Roos-Serote et al. (1995) built a latitude–altitude temperature map. Comparing the results to the Venus International Reference Atmosphere (VIRA, Seiff et al., 1983) significant differences were seen in the 75–80 and 90 km altitude ranges, the NIMS results being respectively some 4 K colder and 10 K warmer than VIRA. VIRA refers to a zonal average and Seiff et al. (1983) give indications of how the temperature field behaves with respect to VIRA as a function of local time. The observed differences in the 75–80 km altitude range can tentatively be explained in terms of thermal tides. However, this does not work for the higher temperatures at 90 km altitude. Clearly more data (at other local times) are needed to address this issue; with VIRTIS we plan to measure the local time–latitude–altitude temperature map for the night side hemisphere of Venus every 10 days. We will be able to measure and track any tides and other waves that might exist.

From the altitude–latitude map obtained from NIMS, and assuming cyclostrophic balance, Roos-Serote et al. (1995) then inferred the zonal winds as a function of altitude and latitude. This is the only way the winds can be derived from remote sensing in this altitude range, as no cloud features are available here to track wind speeds. The wind speed at the cloud tops provides the boundary condition to integrate the thermal wind equation. In this analysis, it was taken from measurements made on the dayside of the planet by the Solid State Imaging instrument aboard Galileo. They found that the wind generally decreases with altitude. They found jets with speed of $-105 \, \text{m s}^{-1}$ centred at $-30°$ and $+20°$ latitude and 70 and 75 km altitude, respectively. With VIRTIS is will be possible to determine the wind field above the clouds in a much more systematic and accurate way using this technique.

3.3. Radiative transfer in the upper atmosphere

Radiative transfer is a key component of the energy balance, thermal structure and dynamics of the upper atmosphere of Venus. The mesosphere, from the cloud tops to about 110 km (0.01 nb) is controlled by strong convection in the lowest layers and by weak radiative losses in the infrared, as the CO_2 bands are optically thick (VIRA model, Seiff et al., 1985). Minor absorbers like SO_2 and H_2O, and scattering and absorption in the UV by aerosols do have a contribution, but only below 75 km (Haus and Goering, 1990). The Pioneer Venus and Venera missions, and more recently Galileo, sounded this region in the UV and in the IR spectral ranges. They found latitudinal variations in the thermal structure indicative of a region in cyclostrophic balance (Taylor et al., 1983; Roos-Serote et al., 1995) with significant solar thermal tides (Schofield and Taylor, 1983) and gravity wave signatures (Seiff et al., 1992; Hinson and Jenkins, 1993). Above about 110 km, in the thermosphere, in addition to UV solar heating and thermal conduction, the infrared absorptions and emissions by CO_2 are crucial for understanding the energy balance. CO_2 is known to be in non-local thermodynamical

equilibrium (non-LTE) at these altitudes. These conditions normally take place at low pressures, when molecular collisions cannot redistribute efficiently the internal energy of the atmosphere among the different modes (translational and vibrational energy of the different molecules, for example). As a consequence, the CO_2 energy states are not populated according to Boltzmann statistics but rather follow an a priori unknown function. Specific theoretical calculations are required to solve the problem, which needs to be coupled to the usual radiative transfer problem, in a typical example of radiation-matter non-linear interaction. The pioneering work by R. Dickinson more than 30 years ago (Dickinson, 1972) pointed out an additional difficulty in a thick CO_2 atmosphere such as on Venus: weak lines play a key role in the transport of radiation in the wings of the strong lines. Therefore, the number of bands to consider for a proper representation of the energy states and of the radiation field is very large.

A comprehensive non-LTE model for CO_2 emissions in the Venus upper atmosphere was recently developed by Roldan et al. (2000), following previous models for the Martian atmosphere by the same group. They obtained daytime and night time populations for the most relevant CO_2 levels emitting in the infrared, which can then be used to compute radiances emerging from the Venus upper atmosphere (see below). They also computed the thermal cooling rates at 15 μm and the solar absorption in the near-IR range (1–5 μm), which dominate the atmospheric radiative balance in the upper mesosphere and lower thermosphere. Although the original model of Roldan et al. (2000) did not include CO vibrational states, these have been recently added to the model following a similar scheme to the Martian model, and allowing for the efficient exchange of vibrational excitation with CO_2 states (Lopez-Valverde et al., 2007). The predictions from this non-LTE model are of course subject to a number of uncertainties, including unknown rate coefficients for some collisional exchanges and a number of approximations to the radiative transfer problem. Obviously, an ideal validation strategy would be to compare with suitable infrared measurements from orbiting satellites, but these are scarce so far.

There is, therefore, a strong need to contrast all these theoretical predictions against real data, in order to gain confidence in our understanding of the physics of the Venus thermosphere. VIRTIS may supply a wealth of data to learn about key non-LTE processes in Venus, as it will sound the most important CO_2 and CO emissions in the infrared, those around 2.7, 4.3 and 4.7 μm, all of them subject to strong non-LTE situations, and in addition, strongly coupled between them.

Our numerical simulations using this non-LTE model indicate that VIRTIS should be able to detect the strong non-LTE emission from CO_2 in the 4.3 μm region during daytime in both nadir and limb sounding, and with both M and H modes. The H mode should be more useful, as it may allow us to separate contributions from different bands (fundamental from hot bands, and also between different CO_2 isotopes), and therefore, to test the collisional exchanges between the different CO_2 states, each one populated by different physical mechanisms. The 2.7-μm CO_2 emissions should easily be detected at nadir, whereas they would not be under LTE conditions. The CO 4-μm fundamental band also presents a nadir LTE (or night time) signal about one order of magnitude lower than the non-LTE daytime emission, but still detectable with VIRTIS M and H modes. The expectations for these bands in limb sounding with the H-mode are particularly promising, with detection being possible up to 160 km at least. In addition, the H-mode will allow observation of the individual lines of the CO band, providing information about the rotational temperature up to the upper thermosphere. These CO_2 and CO non-LTE emissions will hopefully be correlated and complemented with PFS observations, which employ different resolutions and field of view.

Oxygen airglow is another non-thermal emission traditionally used to study the upper atmosphere of the terrestrial planets. Of particular interest is the O_2 infrared band at 1.27 μm, detected in the Venus atmosphere by ground-based telescopes (Connes et al., 1979; Crisp et al., 1991). In Earth's upper atmosphere, this emission originates from the photolysis of ozone (dayglow) followed by three-body recombination of atomic oxygen (day and nightglow). On Venus, the production mechanism most likely originates from the photolysis of CO_2 at thermospheric altitudes followed by both large-scale horizontal transport to the night side and downward transport of atomic oxygen to lower layers. Then, in the upper mesosphere (95–110 km), three-body recombination to excited O_2 (Allen et al., 1992; Bougher and Borucki, 1994) produces the airglow. This general picture contains, however, a number of intriguing facts. First, the strong intensity observed seems to suggest an almost complete efficiency for conversion of CO_2 photolysis to excited O_2 ($a^1\Delta_g$). Secondly, the similar intensities observed on the night side and day side (Connes et al., 1979) suggest that atomic oxygen can travel very efficiently to the night side, without losses, which represents a photochemical problem not fully solved (Slanger and Wolven, 2002). In addition, Crisp et al. (1996) found this band system to show a strong variability over very short time and spatial scales, which could be related to changes in the downwelling branch of the global circulation pattern from the dayside to the night side hemisphere. Similar arguments were used by Drossart et al. (1993) to explain variable intensities in NIMS/Galileo data. Also, gravity waves generated at the cloud top could be responsible for additional changes in these emissions (Bougher and Borucki, 1994).

VIRTIS will hopefully shed light on all these questions. Based on previous measurements and models, we estimated that VIRTIS should detect the O_2 1.27-μm limb emission during daytime, while during night time VIRTIS will detect it in both nadir and limb observations. The nadir and limb observations and their higher spatial resolution will help to

monitor the spatial and temporal variability and to analyse for the first time the vertical profile of this emission.

3.4. The influence of the presence of sulphuric acid aerosols on radiance spectra of Venus

The aerosols act as efficient scattering centres by modifying the planetary albedo for solar radiation and by absorbing the upward thermal radiation, which is partly re-emitted. The solar reflection can be either increased (for nonabsorbing aerosols above a low-reflecting ground) or decreased (for absorbing aerosols above high-reflecting ground). On the global scale, the planetary albedo most likely increases with any increase of the aerosol loading and leads to change the temperature of the ground. The issue of a cooling role for the aerosols is still open. Sulphuric acid (H_2SO_4) aerosol was found to be the primary chemical constituent of the clouds on Venus. These aerosols are concentrated in the main cloud at altitudes of about 48–70 km, in the subclouds at ∼48–35 km) and also in the precloud (∼70–90 km) hazes.

Satellite monitoring of aerosol properties using passive techniques is widely considered to be a crucial tool for the study of the nature of aerosols and their optical and climatic effects. With VIRTIS, the radiation reflected and emitted from the surface and clouds on Venus can be analysed in the spectral range 0.25–5.0 μm. Simulations of the radiance above the atmosphere are necessary to understand the atmospheric optical processes, the structure of the clouds, and to facilitate the interpretation of the data measured from Venusian orbit. To calculate the bidirectional radiance—which is the quantity measured by the VIRTIS spectrometer—two contributions to the signal have to be taken into consideration. The first is the surface contribution, which depends on surface reflectance and emittance, the second is the signal from the atmosphere, which depends on the thermodynamical parameters of each layer and of the densities of gases and aerosols. We consider the solar radiance reflected from the Venusian surface and scattered in the atmosphere, and the radiance thermally reemitted from the surface and from the particles and molecules in the atmosphere. All radiation is transmitted and filtered through the atmosphere on its way to the receiver. The parameters of the atmosphere, density of aerosols and gases change from layer to layer which causes of course the differences in transmittance at various altitudes.

Calculations with representative atmospheric models of Venus are being prepared for the interpretation of VIRTIS data. The transmittance, reflectance and emittance from various atmospheric layers are calculated separately and then combined. The light-scattering and absorption coefficients are computed for model aerosol clouds for a range of wavelengths and various microphysical properties of the particles (Blecka, 1999; Blecka and Erard, 2004). Aerosols are computed using the spectral index of refraction (n, k) of 75% H_2SO_4. The size distribution of aerosols is a lognormal distribution in which the values of parameters depend on the mode of the cloud (Revercomb et al., 1985). The Mie code (from Bohren and Hufmann, 1983) modified for lognormal size distribution is used in the computation of optical properties, assuming spherical particles. The aerosol and gas contributions to the total radiance is accounted for by computing absorption, single and multiple scattering, and emission in the direction of observation.

In the models the aerosols of Venus can be represented by three main modes, the first of which contains submicron particles, apparently present in both the upper cloud layer and the subcloud haze. Sulphuric acid droplets with mean radius $r = 1$ μm, representing the principal second mode, are responsible for the formation of clouds and populate mainly their middle layer near 55 km altitude. The third mode, present in the lower layer, near 50 km altitude, is made up of the relatively small number of the coarsest fraction of these particles, bigger in size (Marov and Shari, 1997). Validation of these models will be a goal of the interpretation of VIRTIS data.

4. Surface science with VIRTIS

Our existing knowledge concerning the surface of Venus comes primarily from extensive radar imaging of the planet and from a limited number of surface images and other information obtained by the series of Venera landers. Radar imaging of the planet, showing mountains, craters, and plains, has been performed both from Earth-based facilities and from space probes such as Magellan. Most of the rock is probably basalt, which is typical of volcanism. Venera 8, which landed on a cratered, ancient plain southeast of the Beta Regio volcanic complex, reported an analysis that reflects a surface composition similar to an extreme alkali basalt or granite. Little information about the mineralogical composition of the soil of Venus has been obtained so far, and, in particular, there have only been suggestions about the abundances of the oxides SiO_2, Al_2O_3, MgO, CaO, FeO, K_2O, etc. (see Table 2).

The real oxidation state of the surface is unknown, but the composition of the atmosphere can help us introduce constraints. For instance, suggestions that the atmospheric abundances of all the reactive gases on Venus, including

Table 2
Major-element composition (wt %) of the Crust of Venus

Oxide	Venera 13	Venera 14	Vega 2
SiO_2	45.1	48.7	45.6
Al_2O_3	15.8	17.9	16.0
MgO	11.4	8.1	11.5
CaO	7.1	10.3	7.5
FeO	9.3	8.8	7.7
K_2O	4.0	0.2	0.1
TiO_2	1.6	1.2	0.2
SO_3	1.6	0.9	4.7
MnO	0.2	0.2	0.1

oxygen, carbon dioxide, hydrochloric and hydrofluoric acid, and the sulphur compounds, are regulated by buffer reactions with crustal minerals, mean that the iron oxidation can be discussed via the relative abundances of CO and CO_2 as indicators of the oxidation state of the atmosphere. Under equilibrium conditions of temperature and pressure the reaction: $Fe + CO_2 \rightarrow FeO + CO$ would permit solid metallic iron and pure FeO (or FeO-rich pyroxene). The FeO/magnetite boundary would be determined by the reaction $3FeO + CO_2 \rightarrow 3Fe_3O_4 + CO$. In this case, observing the CO mole fraction in the atmosphere potentially can provide some information about this surface chemistry and the mineralogical components present. The oxidization of magnetite to haematite via $2Fe_3O_4 + CO_2 \rightarrow 3Fe_2O_3 + CO$ can also be analysed through observations of the amount of CO.

The chemical composition of the lower atmosphere, in particular the CO/CO_2 and COS mixing ratio, is crucial to understanding the effects of chemical weathering on the surface of Venus. Dramatic changes in radar emissivity values have been observed by Magellan above high relief (>5000 m above MPR) and have been interpreted as due to chemical weathering of the surface basalt operated by the atmosphere at high altitudes (Pettengill et al., 1992). The mineral responsible for low emissivity on mountain tops and volcano edifices appears to be the electrical semiconductor pyrite, whereas magnetite is thought to characterize the lower altitude (Klose et al., 1992). In addition, available data suggest that magnetite and haematite may both be stable on the surface, probably in solid solution with other oxide minerals.

Interestingly, Maat Mons volcano, which reaches ~6000 m in height, does not show this low emissivity at the summit. This has been interpreted as possible evidence for recent volcanic activity, which prevented the weathering effect at high altitude (Klose et al., 1992; Robinson et al., 1995).

The altitudes at which the magnetite/pyrite phase boundary is encountered vary with the redox state (CO/CO_2 ratio) of the troposphere, which is still poorly known (Fegley et al., 1997; Wood, 1997). Radar data cannot provide constraints on the mineral stability under corrosive conditions, but spectral mapping by VIRTIS of the near-surface can define the redox state of the atmosphere and thus identify the surface minerals in equilibrium with the atmosphere. In combination with the surface classification, this might help to distinguish, for example, between surface material flowing out of the volcano and the weathered material that is being covered up.

The Magellan images have shown that Venus has been among the most geologically active planets in the Solar System. Volcanism and tectonics strongly shaped the surface (Solomon et al., 1992). Large lowlands cover about 80% of the surface and highly deformed plateau (tesserae) form the highlands. While there is evidence that the majority of the observed tectonic and volcanic features of Venus formed in a short period of time close to 500 Myr

ago, regional and global stratigraphy studies based on Magellan images pointed out that volcanic activity has shaped the surface in different geological epochs and may still be active in recent times (Basilevsky et al., 1997; Basilevsky and Head, 2002; Guest and Stofan, 1999). Dating of the recent resurfacing activity on Venus, based on impact crater density, confirms that some of the volcanic units are among the youngest geological features (Strom et al., 1994; Price et al., 1996; Basilevsky and Head, 2002).

Regarding the mineralogical composition of the surface of Venus, we actually know quite reliably that the plains covering 75–80% of the surface are generally basaltic. However, we do not know, in most cases, what types of basalts make up the tesserae, steep-sided domes, etc. Moreover, the observation on Magellan images of sinuous and long *canali*-type channels suggests unusual lava process occurring locally on Venus, involving very low-viscosity lavas (Baker et al., 1992; Komatsu et al., 1993) which are rare on Earth.

The M channel of VIRTIS will allow the first systematic mapping of the surface and near-surface atmosphere of Venus in the near infrared atmospheric windows located at 1.10, 1.18 μm and possibly at 1.02 μm (Wattson and Rothman, 1986; Kamp et al., 1988; Moroz, 2002). The last of these is unfortunately right at the low end of the wavelength range of the IR channel and at the upper end of the VIS channel, so the usability of this window is unclear until the first data from Venus are obtained. The atmospheric windows will allow measuring the thermal emission of the surface as was demonstrated by Galileo/NIMS (Carlson et al., 1991) and Cassini/VIMS (Baines et al., 2000). Based on these data three main science tasks for the surface analysis will be pursued: Classification of the surface composition, studies of the interaction between low atmosphere and surface, and mapping of the variability of the surface temperature.

To first order, the surface temperature on Venus is simply a function of altitude with a temperature lapse rate of 8 K/km (Seiff et al., 1985; Meadows and Crisp, 1996). Therefore, the thermal emission from the surface measured in the NIR atmospheric windows is a function of the topography. This was nicely shown by the comparison of Galileo/NIMS observations and Pioneer Venus altimetry (Carlson et al., 1991). For the first phase of the mission, surface temperature and its spatial distribution will be predicted using the temperature lapse rate of 8 K/km and the Magellan topography, for comparison to the surface emission measured by VIRTIS in the atmospheric windows. In a later stage of the mission the temperature lapse rate and the near surface atmospheric temperature will be derived directly from the VIRTIS and PFS measurements, along with an estimate for the emissivity of the surface for each of the wavelengths. While these windows have a relatively high transmittance of 40–95%, the cloud deck complicates the observations. Multiple reflections between the surface and the clouds tend to wash out the contrast

between high albedo and low albedo parts of the spectrum. This puts constraints on the achievable contrast for the surface emissivity, as discussed by Baines et al. (2000). However, Hashimoto et al. (2004) have put forward an improved method to deal with these effects and have applied it successfully to the Galileo/NIMS observations. The estimations show an achievable emissivity contrast of at least $(\varepsilon_2-\varepsilon_1)/\varepsilon_1 = 0.17$ (Hashimoto and Sugita, 2003). A similar correction algorithm will be used for the processing of VIRTIS data to remove atmospherically and topographically induced contrasts in the bands located close to the atmospheric windows, leaving contrasts due to compositional variability or unexpected temperature variation of the surface. The data processing steps necessary to extract the surface information are:

- Removal of scattered sunlight.
- Binning of the relevant image planes into images centred at 1.02, 1.10, 1.18, 1.27 and 1.31 μm.
- Correction for limb darkening.
- Removal of cloud contrasts using the windows at 1.27 or 1.31 μm.
- Removal of topographic contrasts with synthetic radiance images based on surface temperatures derived from Magellan topography data.
- Correction for multiple cloud–surface reflections.

The algorithm developed for the determination of absolute surface emissivity values needs very little computing time and can handle the expected large amount of VIRTIS-M Venus night side data.

Based on the derived surface emissivities a classification map of surface types can be produced. The achievable spectral contrast should allow identifying variation in the FeO content from the 1.10 and 1.18 μm windows. From this it will be possible to map the distribution of mafic and felsic material on the surface (Rogers and Hawkesworth, 2000). The classification map derived from the VIRTIS measurements will complement the radar reflectivity and radio-thermal emissivity derived from Magellan and Pioneer data sets and provide crucial information on the surface composition and its spatial variation.

Should Venus still have active volcanism at the surface this would lead to a localized excess of thermal radiation on the surface. Based on the instrument performance an increase by 10% in the thermal radiation from the surface can be identified. Following the estimates by Hashimoto et al. (2001), VIRTIS should be able to detect lava flows with a surface temperature of at least 1000 K if they cover an area larger than approximately 20 km². This flow dimension is in the lower range of lava flows observed by the radar images obtained by Pioneer Venus and Magellan: typical dimensions are several tens of kilometres in length and several kilometres in width (Zimbelman, 1998). Small lava lakes covering an area of less than 1 km² are detectable if the surface temperature exceeds 1200 K; liquidus temperatures for basalt of up to 1500 K can be expected.

Estimates on the lava cooling rate by Head et al. (1986) indicate that an eruption would be undetectable after one Earth day. This implies that the chance of detecting volcanism increases if the time between surface observations of the same location is small. Of special interest here are the maps obtained from the apocenter mosaic observations. While each of the maps can be analysed separately for excess radiation indicating volcanic activity, analysing the differences between successive maps might be an even more sensitive tool. Unfortunately, the results obtainable will not be unambiguous because of variations within the cloud structure. Therefore, a careful correlation of possible eruption events with surface morphology is necessary. Further confirmation can be derived from an analysis of the near surface atmosphere composition, since volcanic activity should produce a localized increase of gas emission (CO_2, CO, SO_2, HF, CH_4).

Observations for surface studies will be obtained mainly on the night side of the planet. During dayside observations, the contribution of the thermal emission from the surface will most likely be washed out by the thermal emission from the atmosphere and the cloud particles. As discussed by Moroz (2002), this will make measurements of emissivity variations on the surface rather difficult. It is planned to perform targeted observations for surface studies during the descending branch of the orbit, and mapping observations during the apocenter mosaic mode. Given the orbital velocity of the spacecraft, VIRTIS-M can obtain multispectra images using the pushbroom mode only for altitudes large than approximately 10,000 km; below this altitude there will be gaps between the individual stripes. The best obtainable spatial resolution from an altitude of 10,000 km will be about 16 km, while during the pericenter pass the spatial resolution will be better than 1 km. This is however an unrealistic value, because any photon being emitted from the surface will encounter multiple scattering by particles in the clouds, resulting in blurring of the images and limiting the spatial resolution to 50–100 km (Moroz, 2002).

The limitations on achievable spatial resolution and latitudinal coverage put some constrain on the selection of targets, limiting them to features with a diameter larger than 150 km. A typical target for early observations would be Quetzalpetlatl Corona, with a diameter of 780 km. And an altitude difference of more than 2 km within the FOV. Assuming a temperature lapse rate of 8 K/km one would expect a significant difference between the thermal emission from the corona top and the low lying base material. Comparing the derived emissivity of the corona material with the surrounding area will allow a search for possible compositional differences. The fact that VIRTIS covers both areas within the same FOV will reduce possible cross calibration effects.

In the apocenter mosaic mode, maps of the Southern Hemisphere are obtained at regular time intervals. While the spatial resolution is less than for the targeted observations at lower distances, these observations still

have a high scientific value since, as discussed above, repetition of this observation mode over the whole mission lifetime will allow a search for time variability of the surface emissivity. Furthermore, by stacking large numbers of observations the effect of variation in optical thickness of the clouds can be reduced.

The data VIRTIS can provide on the surface of Venus has never been obtained before in a systematic way. While the flybys of Galileo and Cassini have shown that the principle of using atmospheric windows to study surface variations is sound, VIRTIS will do the first systematic survey of the whole Southern Hemisphere surface of Venus, and be the first instrument to routinely monitor the Venusian surface for volcanic activity. An integration of the VIRTIS data set with existing data from radar and from in situ measurements at landing sites will significantly improve our understanding of the evolution of the surface of Venus.

5. Atmospheric dynamics

Fundamental phenomena related to the dynamics of Venus' atmosphere to be observed by VIRTIS include the equatorial super-rotation and the meridional circulation of the atmosphere; the polar vortices; atmospheric thermal structure and radiative balance; atmospheric waves and oscillations; and small-scale motions associated with clouds and convective cells. The VIRTIS data will allow study of the above phenomena in three main ways: (1) temperature mapping, which leads also to indirect derivation of wind magnitudes from the thermal wind equation; (2) direct measurement of winds by tracking of cloud features; and (3) mapping of trace chemical species which are indicative of atmospheric motions. Dedicated observation campaigns are planned for more detailed observation of fine-scale cloud structure, and of the polar vortices.

5.1. Temperature mapping

Using radiance measurements in the 4.3 μm CO_2 band, the temperature field will be retrieved in the altitude region 60–90 km, i.e., from the cloud tops to the base of the thermosphere. Repeated sounding will yield three-dimensional maps of temperature, which, when used as inputs into general circulation models, will lead to an improved understanding of the global circulation in this altitude region. For this purpose, a spatial resolution of around 0.5–3° in both latitude and longitude should be satisfactory. Vertical integration of the thermal wind equation will then enable the derivation of the zonal wind magnitude from the measured latitudinal temperature gradient. From the vertical and latitudinal temperature gradients the Richardson number can be estimated, which is a measure of the susceptibility of the flow to symmetric inertial instability (Andrews et al., 1987).

Repeated observations during consecutive orbits will constrain the temporal variability in the temperature

structure, and in particular make it possible to derive the principal wave modes. Continuous coverage for 10 days or more is needed to cover the larger-scale waves, which will include modes having periods typically longer than 3 days.

Maps of the surface temperature and its variability with elevation will be retrieved using radiance measurements in the 1.0, 1.1 and 1.18 μm window regions and comparing to the known elevations of features as determined previously by Magellan and Pioneer-Venus RADAR experiments. Because of the large range of topography on the surface, this allows the calculation of the lapse rate in the lower atmosphere, which contains information about the vertical stability of the atmosphere in the lowest 10 km (Meadows and Crisp, 1996).

5.2. Clouds tracking and winds retrieval

Repeated images of the same regions with VIRTIS-M will permit the study of cloud evolution and the direct measurement of winds via the cloud-tracking technique. Features located at different altitudes can be identified by the use of multiple wavelengths, including UV and visible images on the dayside (e.g., at 0.3 μm) and near-IR (e.g., at 1.7 and 2.3 μm) on the night side of the planet. In addition to the mean zonal and meridional winds, the wind velocity fluctuations (turbulence) will allow an estimate of the eddy momentum and heat transports in the atmosphere. By observing for long periods over full latitude circles, it will be possible to separate out the mean zonal and transient flow components, and possibly to identify the influence of the surface topography in the generation of atmospheric features such as cloud or flow patterns, including waves. As in the case of temperature measurements, campaigns involving the study of waves should last for at least 7–8 days in order to obtain a minimum of two complete rotations of the atmosphere. Longer campaigns of 20 days or more will be needed to study wave variability, but such a campaign may be done only once during the nominal mission, emphasizing coverage of the night side in order to extract the modes in the deep atmosphere.

Precise mapping of latitudinal gradients in zonal wind jets, combined with momentum transports, should make it possible to establish a link between the mean flow and potential eddy-generating dynamic instabilities. This should be an important measure of the importance of the Gierasch–Rossow mechanism in the maintenance of atmospheric super-rotation (Gierasch, 1975; Rossow, 1983; Rossow and Williams, 1979) relative to other candidate mechanisms, such as a solar thermal tide (Schubert and Young, 1970) or orographically forced waves (Hou and Farrell, 1987). Vertical wind shears, combined with the vertical gradient of potential temperature between 60 and 90 km will also allow an independent estimation of the Richardson number.

Because of the eccentric polar orbit, the sampling of the two hemispheres will be quite different. When above the Northern hemisphere VIRTIS is too close to the planet,

and travelling too fast, to observe the same point in successive images. However, extended coverage will be obtained over most of the Southern Hemisphere, especially for latitudes polewards of 30°. Since the high obliquity of Venus (177°) makes the rotation axis almost perpendicular to the ecliptic, seasonal effects are negligible and it is reasonable to expect symmetry between the Northern and Southern Hemispheres, so that the two categories of coverage can be treated as complementary. Temporal sampling may vary from half-hourly to daily, ensuring that cloud features move at least a few pixels between successive images. These observations, together with the global coverage obtained through the mosaics acquired at apocenter, will allow VIRTIS in particular to monitor the activity of the southern mid-latitude jet, and also to build maps of the cloud-top altitude (dayside), which will constrain the global dynamics above and within the upper cloud layer.

5.3. Chemical tracers

Using night side observations of near-IR atmospheric windows, VIRTIS will retrieve the distribution of several chemical compounds in the deep atmosphere below the clouds. The water vapour vertical profile in the altitude region between the surface and 35 km may be obtained from the 1.18 and 2.3 μm windows. Similarly, CO and OCS will be mapped in the region around 30 km altitude, and SO_2 in the 35–45 km region. A goal is to get the largest possible coverage of the latitudinal distributions of these compounds, in order to establish a relation between latitudinal variations and the meridional circulation. In particular, the CO latitudinal gradient noted in Galileo near IR observations (Collard et al., 1993) may be an indirect signature of the Hadley circulation. Because of the asymmetric coverage of the hemispheres, VIRTIS-M maps will be used for transport studies over the Southern Hemisphere, where complete coverage is foreseen, while VIRTIS-H will permit species retrievals in the 2.3 μm window with maximum spatial and spectral resolution in the northern hemisphere, optimizing the study of cloud chemistry.

Observations of non-LTE emission lines will allow mapping of gas species, which may serve as tracers diagnostic of circulation in the upper atmosphere. Spectral features to be mapped include O_2 nightglow at 1.27 μm, as well as dayside non-LTE emission lines of O_2 (1.27 μm), CO (4.7 μm) and CO_2 (2.7 and 4.3 μm).

5.4. Cloud morphology and convection cells

VIRTIS pictures of cloud morphology, obtained with both high spatial and high spectral resolutions, will show the fine structure of the clouds, in nadir or near-nadir geometry. This is of most interest at low latitudes, where there is evidence at the cloud tops of convective structures in the cloud layer. These structures may have length scales

of order 300 km (Rossow et al., 1980; Toigo et al., 1994), so observations with a spatial resolution of less than 10 km are required to show them in fine detail. The easiest way to obtain these images may be to use push-broom imaging near the top of the ascending branch of the orbit, when the Venus Express spacecraft will be approaching Venus' equatorial region at an altitude of around 10,000 km. Using this mode would result in images with a pixel size of roughly 10×10 km. High spatial resolution images may also be obtained at other latitudes during the ascending branch of the orbit, over the Southern Hemisphere, in order to investigate the evolution of mesoscale structures as a function of latitude. On the dayside, the structure of the cloud tops and the UV absorber distribution will be investigated; on the night side, VIRTIS will probe beneath the cloud tops and perhaps see evidence of convection cells and establish whether any correlation exists between cloud morphology and chemical tracer abundances. Quasi-simultaneous observations of the day–night border (visible–IR) will allow us to study the correlation between the cloud morphology and motions at two levels separated by about one-scale height, and infer their dynamical coupling.

5.5. Polar vortex

Data from Pioneer Venus revealed an enormous (diameter ~5000 km) rotating vortex with a double-eye structure (the polar dipole) and a cold collar at the north pole of Venus (Taylor et al., 1980), and Earth-based observations (e.g., Diner et al., 1976) suggest that a similar phenomenon occurs at the south pole. However, the reasons for its complex spatial and temporal structure are still largely unknown, as are the mechanisms that create this regime, and link it to the global circulation at lower latitudes. Polar vortices, and polar vortex isolation of trace chemical species and temperature, have been identified in the atmospheres of Earth and Mars, and recently Titan as well. Accurate mapping of dynamical variables in Venus' polar vortex will allow a better understanding of the phenomenon, and will constrain models over three different dynamical regimes (the Rossby number grows from 0.1 to 1 and 25, respectively, for the Earth, Titan and Venus).

Taylor (1990) summarised the key observational features of the polar vortex and offered a qualitative theory of its nature and origin. The dipole bears an obscure relationship to the polar collar, a cold (typically more than 40 K below its surroundings) feature that surrounds the dipole at latitudes from 60 to 75°N approximately. Unlike the dipole, the collar does not rotate rapidly and is mainly a temperature, rather than cloud morphology, feature. Also unlike the dipole, which is obviously a feature with a mainly wavenumber two character, the collar is primarily wavenumber one, as can be seen from its crescent-shaped appearance in the images (see figures in Taylor et al., 1980). The linear filaments which are sometimes seen connecting

the opposite cusps of the polar vortex "chevrons" are very difficult to explain, even speculatively.

The rotation of the dipole was measured by Schofield and Diner (1983), who found that the motion had three components which exceeded the measurement error: a steady rotation with a period of $2.945 + 0.003$ days (retrograde); a secular decrease in period with a deceleration of $0.21 + 0.05°$ day^{-1}, and a sinusoidal component with a peak amplitude of $0.39 + 0.06$ and a period of about 40 days. In addition to its variable rotation rate, the dipole also appears to nutate, and varies the position of its axis of rotation with respect to that of the planet. On at least one occasion (Plate 3a in Taylor et al., 1980) the apparent centre of the dipole was observed to be displaced by about $5°$ of latitude, or about 500 km, from the pole.

Elson (1982) was the first to try to model the dipole and found some normal modes that exist under conditions approximating the polar Venusian atmosphere, and in which wavenumber 2 is dominant. The collar may be the manifestation in the temperature field of a jet stream at latitudes between about 50–60°N, which separates the low-latitude from the high-latitude regimes. South of the jet, large amounts of mass and angular momentum are being transported polewards at the cloud-top level; inside the collar this mass and momentum is propagated downwards inside the dipole. Perhaps the rotation rate of the eye of the vortex, and its shape, represent the most stable configuration for conserving mass and angular momentum during this process.

It is impossible even to describe, let alone explain, the vortex and its behaviour completely using the short (72-day) Pioneer Venus data set. From Venus Express, the southern dipole will first be conclusively identified and characterized by maps of its temperature fields, cloud opacity and trace gases using repeated mosaics obtained at apocenter over 7–11 consecutive orbits (corresponding to 2–3 rotations of the vortex). For the northern polar vortex, repeated nadir observations during successive pericenter passes will allow VIRTIS to obtain meridional profiles of the polar vortex structure, in the form of temperatures and trace gas abundances. Since the rotation period of the vortex, and its position relative to the pole as well as its detailed morphology, all vary with periods ranging from short (about 1 day) and long (several years), the most realistic strategy to get a full view of the vortex structure and behaviour is through campaigns of 10 consecutive days, repeated at least every 100 days throughout the mission.

6. Tentative observations

6.1. Seismology

The interiors of the planets are mechanically coupled to their atmospheres through the surface. On Earth, atmospheric signals created by ground movements have been detected and imaged just above the quakes (Kelley et al., 1985; Calais and Minster, 1995) and, far from the event, above seismic surface waves (Ducic et al., 2003; Artru et al., 2004; Garcia et al., 2005a). The ground vibrations generate acoustic and gravity waves that propagate upward in the atmosphere; if we neglect dissipation mechanisms, the kinetic energy is conserved during their upward propagation, creating an exponential increase of their amplitude due to the exponential decrease of atmospheric density. On Earth, the amplification factor attains ~10,000 at 150 km altitude. Because of the higher atmospheric density and pressure at the surface and a lower impedance contrast at the ground–atmosphere interface, the coupling between the ground and the atmosphere on Venus is about 600 times greater than on Earth. Thus, the (probably) weaker seismic activity on Venus is counterbalanced, compared to the Earth, by better atmospheric coupling, a unique situation in the solar system.

Recent computations (Garcia et al., 2005b) have quantified the temperature and density perturbations expected to be created by quakes in the upper atmosphere of Venus. These perturbations can be divided in two types: a local temperature increase above the source due to the mechanical energy dissipation in the upper atmosphere, and adiabatic temperature and density perturbations created by acoustic waves. Fig. 4 presents the upper atmosphere temperature perturbations due to these two effects above a reverse-fault earthquake of magnitude 6.0 (Garcia et al., 2005b). The expected perturbations are significant for altitudes above 130 km.

VIRTIS-M will recover upper-atmosphere local temperature increases above quakes using mosaics formed by repeated along-track measurements of a specific point for more than 2000 s. From these it may be possible to recover atmospheric acoustic modes via a spectral analysis of the
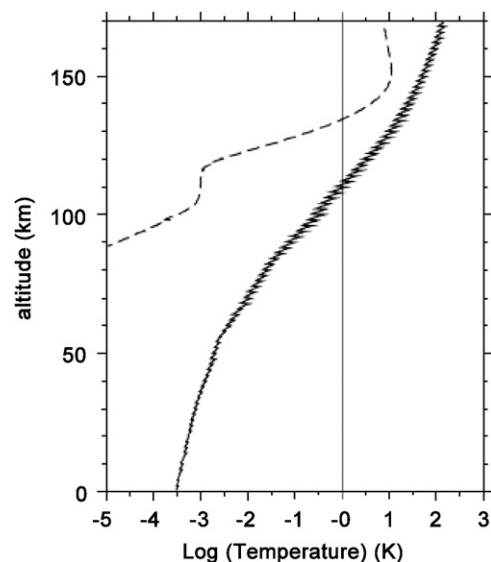

Fig. 4. Average local temperature increase (dashed line) and amplitude of adiabatic temperature perturbations (plain line) in the atmosphere of Venus above a reverse fault quake of magnitude 6.0. Extracted from the computations of Garcia et al. (2005b).

molecular emissions and absorptions in the upper atmosphere of Venus, although the effect of temperature and density perturbations on these emissions and absorptions are still to be studied. While these measurements are quite challenging, the detection of Venus quakes and/or atmospheric acoustic modes can bring new constraints on Venus tectonics and interior structure.

6.2. Lightning

A search for lightning activity on the night side of Venus is possible using long integration times in the visible channel of VIRTIS-M, offering the chance to settle a long and controversial argument involving contradictory results between major spacecraft-borne experiments (Hunten, 1995). Pioneer Venus imaging observations by (Borucki et al., 1991), did not provided a positive detection of lightning, while the radio wave experiment on Galileo apparently did (Gurnett et al., 1991). The most stringent non-detection limit for lightning on Venus came from the Cassini flyby (Gurnett et al., 2001). Lightning can be detected by whistler-mode detection at radio wavelengths or by detecting direct emission in the visible or near infrared. On Jupiter, such activity has been well observed, in particular by Galileo, and even related to specific features, probably water clouds (Little et al., 1999).

Even if conventional storm lightning activity is not plausible on Venus (because, for example, charge separation is not expected to be as great in H_2SO_4 clouds as in H_2O clouds), different phenomena could nevertheless be present on Venus, such as cloud-to-cloud or cloud-to-ionosphere discharges, which could induce signatures in the radio wave experiments. Despite the fact that VIRTIS, as a long slit spectrometer, affords observations of only a small area on the planet at one time, valuable information on lightning spectral characteristics can still be obtained with careful planning. For example, non-targeted observations on the night side (mostly after dusk where the probability of lightning has been suggested to be higher) can be performed on a regular basis to search for spectral evidence, which would escape wide filter imaging observations.

6.3. Volcanic activity

The direct detection of volcanic activity is possible with a remote-sensing imaging spectrometer, as exemplified by the extensive work of NIMS/Galileo on Io (Lopes-Gautier et al., 1999). As discussed above, the presence of high temperature lava at the surface of Venus may be very brief, as a crust is expected to form rapidly above any lava. Indeed, the absence of detection by Magellan yields some constraints on the existence of "Io-like" activity on Venus. The most sensitive detection could come from subtle variations in atmospheric composition above volcanic plumes or geysers: H_2O or SO_2 concentrations could be modified above the volcanic emitting area, and the high

sensitivity of VIRTIS in night side observations at 2.3 μm (combining VIRTIS-M and VIRTIS-H observations) could detect variations by 10% on areas of the order of 30 km × 30 km. Therefore, systematic surveys of possible anomalies in atmospheric composition will be made, in particular above volcanic regions of Venus.

7. Conclusion and perspectives

At the eve of the Venus Express observations, VIRTIS has been shown to be a very versatile instrument, which will address many different scientific objectives. Some will need well prepared, dedicated campaigns, for studying the dynamics of local features; others will be done by accumulating statistics on Venus following the completion of the Venus Express mission, and all should build on discoveries from previous ground-based and space observations. VIRTIS has also the capacity to discover entirely new features, due to its large spectral and spatial coverage, and reveal new aspects of Venus beyond the current textbook descriptions.

References

Afanasenko, T.S., Rodin, A.V., 2005. The effect of collisional line broadening on the spectrum and fluxes of thermal radiation in the lower atmosphere of Venus. Solar System Res. 39, 187–198.

Allen, D.A., Crawford, J.W., 1984. Cloud structure on the dark side of Venus. Nature 307, 222–224.

Allen, D., Crisp, D., Meadows, V., 1992. Variable oxygen airglow on Venus as a probe of atmospheric dynamics. Nature 359, 516–519.

Andrews, D.G., Holton, J.R., Leovy, C.B., 1987. Middle Atmosphere Dynamics. Academic Press, New York.

Artru, J., Farges, T., Lognonné, P., 2004. Acoustic waves generated from seismic surface waves: propagation properties determined from Doppler sounding observation and normal-modes modeling. Geophys. J. Int. 158, 1067–1077.

Baines, K.H., Bellucci, G., Bibring, J.-P., Brown, R.H., Buratti, B.J., Bussoletti, E., Capaccioni, F., Cerroni, P., Clark, R.N., Coradini, A., Cruikshank, D.P., Drossart, P., Formisano, V., Jaumann, R., Langevin, Y., Matson, D.L., McCord, T.B., Mennella, V., Nelson, R.M., Nicholson, P.D., Sicardy, B., Sotin, C., Hansen, G.B., Aiello, J.J., Amici, S., 2000. Detection of sub-micron radiation from the surface of Venus by Cassini/VIMS. Icarus 148, 307–311.

Baker, V.R., Komatsu, G., Parker, T.J., Gulick, V.C., Kargel, J.S., Lewis, J.S., 1992. Channels and valleys on Venus: preliminary analysis of Magellan data. J. Geophys. Res. 97, 13421–13444.

Basilevsky, A.T., Head, J.W., 2002. On rates and styles of late volcanism and rifting on Venus. J. Geophys. Res. 107.

Basilevsky, A.T., Head, J.W., Shaber, G.G., Strom, R.G., 1997. The resurfacing history of Venus. In: Bougher, S.W., Hunten, D.M., Philips, R.J. (Eds.), Venus II. Arizona University Press, Tucson, AZ.

Bell, J., et al., 1991. Spectroscopic observations of bright and dark emission features on the night side of Venus. Science 252, 1293–1296.

Belton, M.J.S., et al., 1991. Images from Galileo of the Venus cloud deck. Science 253, 1531–1536.

Bézard, B., de Bergh, C., Crisp, D., Maillard, J.-P., 1990. The deep atmosphere of Venus revealed by high-resolution night-side spectra. Nature 345, 508–511.

Bibring, J.-P., Langevin, Y., Gendrin, A., Gondet, B., Poulet, F., Berthé, M., Soufflot, A., Arvidson, R., Mangold, N., Mustard, J., Drossart, P., 2005. Mars surface diversity as revealed by the OMEGA/Mars express observations. Science 307 (5715), 1576–1581.

Blecka, M.I., 1999. A Study of the influence of of the surface emittance and extinction by dust on Martian IR spectra. Adv. Space Res. 23 (9), 1613–1623.

Blecka, M.I., Erard, S., 2004. Numerical simulation of the near infrared radiance of Mars: effects of atmospheric scattering. Adv. Space Res. 34, 1683–1689.

Bohren, C.E., Hufmann, D.R., 1983. Absorption and Scattering of Light by Small Particles. Wiley, New York.

Borucki, W.J., Dyer, J.W., Phillips, J.R., Pham, P., 1991. Pioneer Venus Orbiter search for Venusian lightning. J. Geophys. Res. 96, 11,033–11,043.

Bougher, S.W., Borucki, W.J., 1994. Venus O_2 visible and IR nightglow: implications for lower thermosphere dynamics and chemistry. J. Geophys. Res. 99, 3759–3776.

Brown, R.H., Baines, K.H., Bellucci, G., Bibring, J.-P., Buratti, B.J., Capaccioni, F., Cerroni, P., Clark, R.N., Coradini, A., Cruikshank, D.P., Drossart, P., Formisano, V., Jaumann, R., Langevin, Y., Matson, D.L., McCord, T.B., Mennella, V., Miller, E., Nelson, R.M., Nicholson, P.D., Sicardy, B., Sotin, C., 2004. The Cassini Visual and Infrared Mapping Spectrometer (VIMS). Invest. Space Sci. Rev. 115, 111–168.

Bullock, M.A., Grinspoon, D.H., 2001. The recent evolution of climate on Venus. Icarus 150, 19–37.

Burch, D.F., Gryvnak, D.A., 1971. Absorption of Infrared Radiant Energy by CO_2 and H_2O: absorption by CO_2 between 1100 and 1835 cm^{-1} (9.1–5.5 μm). J. Opt. Soc. Am 61, 499–503.

Calais, E., Minster, B., 1995. GPS detection of ionospheric perturbations following the January 17, 1994, Northridge earthquake. Geophys. Res. Lett. 22, 1045–1048.

Carlson, R.W., Taylor, F.W., 1993. The Galileo encounter with Venus: results from the Near-Infrared Mapping Spectrometer. Planet. Space Sci. 41, 475–476.

Carlson, R.W., Baines, K.H., Kamp, L.W., Weissman, P.R., Smythe, W.D., Ocampo, A.C., Johnson, T.V., Matson, D.L., Pollack, J.B., Grinspoon, D., 1991. Galileo infrared imaging spectroscopy measurements at Venus. Science 253, 1541–1548.

Carlson, R.W., Weissman, P.R., Smythe, W.D., Mahoney, J.C., 1992. Near-Infrared Mapping Spectrometer experiment on Galileo. Space Sci. Rev. 60, 457–502.

Collard, A.D., Taylor, F.W., Calcutt, S.B., Carlson, R.W., Kamp, L., Baines, K., Encrenaz, Th., Drossart, P., Lellouch, E., Bézard, B., 1993. Latitudinal distribution of carbon monoxide in the deep atmosphere of Venus. Planet. Space Sci. 41 (7), 487–494.

Connes, P., Connes, J., Kaplan, L.D., Benedict, W.S., 1968. Carbon monoxide in the Venus atmosphere. Astrophys. J. 152, 731–743.

Connes, P., Noxon, J.F., Traub, W.A., Carleton, N.P., 1979. $O_2(^1\Delta)$ emission in the day and night airglow of Venus. Astrophys. J. 233, L29–L32.

Coradini, A., Capaccioni, F., Drossart, P., Semery, A., Arnold, G., Schade, U., 1999. Virtis: the Imaging Spectrometer of the Rosetta Mission. Adv. Space Res. 24, 1105–1114.

Crisp, D., Allen, D.A., Grinspoon, D.H., Pollack, J.B., 1991. The dark side of Venus: near-infrared images and spectra from the Anglo-Australian Observatory. Science 253, 1263–1266.

Crisp, D., Meadows, V.S., Bézard, B., de Bergh, C., Maillard, J.-P., Mills, F.P., 1996. Ground-based near-infrared observations of the Venus nightside: 1.27-μm $O_2(a^1\Delta_g)$ airglow from the upper atmosphere. J. Geophys. Res. 101, 4577–4593.

de Bergh, C., Bézard, B., Crisp, D., Maillard, J.-P., Owen, T., Pollack, J., Grinspoon, D., 1995. Water in the deep atmosphere of Venus from high-resolution spectra of the night side. Adv. Space Res. 15 (4), 79–88.

Dickinson, R.E., 1972. Infrared heating and cooling in the Venusian mesosphere. J. Atmos. Sci. 29, 1531–1556.

Diner, D.J., Westphal, J.A., Schloerb, F.P., 1976. Infrared Imaging of Venus: 8–14 micrometers. Icarus 27, 191–196.

Drossart, P., et al., 1993. Search for spatial variations of the H_2O abundance in the lower atmosphere of Venus from NIMS Galileo. Planet. Space Sci. 41, 495–504.

Ducic, V., Artru, J., Lognonné, P., 2003. Ionospheric remote sensing of the Denali earthquake Rayleigh surface waves. Geophys. Res. Lett. 30.

Elson, L.S., 1982. Wave instability in the polar region of Venus. J. Atmos. Sci. 39, 2356–2362.

Fegley, B.J., Zolotov, M.Y., Lodders, K., 1997. The oxidation state of the lower atmosphere and surface of Venus. Planet. Space Sci. 125, 416–439.

Filippov, N.N., Tonkov, M.V., 1996. Line mixing in the infrared spectra of simple gases at moderate and high densities. Spectrochim. Acta Part A 52, 901–918.

Filippov, N.N., Tonkov, M.V., 1998. Kinetic theory of band shapes in molecular spectra of gases: application to band wings. J. Chem. Phys. 108, 3608–3619.

Ford, P.G., 1991. MIT-MGN-GxDR SIS records. Global altimetry and radiometry data records (PDS software interface specifications). Internal PDS Report.

Garcia, R., Crespon, F., Ducic, V., Lognonné, P., 2005a. Three-dimensional ionospheric tomography of post-seismic perturbations produced by the Denali earthquake from GPS data. Geophys. J. Int. 163, 1049–1064.

Garcia, R., Lognonné, P., Bonnin, X., 2005b. Detecting atmospheric perturbations produced by Venus quakes. Geophys. Res. Lett 32, 16205.

Gierasch, P.J., 1975. Meridional circulation and the maintenance of the Venus atmospheric rotation. J. Atmos. Sci. 32, 1038–1044.

González, R.C., Woods, R.E., 2002. Digital Image Processing. Prentice-Hall, Englewood Cliffs, NJ.

Guest, J.E., Stofan, E.R., 1999. A new view of the stratigraphic history of Venus. Icarus 139, 55–66.

Gurnett, D.A., Zarka, P., Manning, R., Kurth, W.S., Hospodarsky, G.B., Averkamp, T.F., Kaiser, M.L., Farrell, W.M., 2001. Non-detection at Venus of high-frequency radio signals characteristic of terrestrial lightning. Nature 409, 313–315.

Hashimoto, G.L., Sugita, S., 2003. On observing the compositional variability of the surface of Venus using nightside near-infrared thermal radiation. J. Geophys. Res. 108, 13-1.

Hashimoto, G.L., Imamura, Takeshi, 2001. Elucidating the rate of volcanism on Venus: detection of lava eruptions using near-infrared observations. Icarus 154, 239–243.

Hashimoto, G.L., Roos-Serote, M., Sugita, S., 2004. Variations in Near-Infrared Emissivity of Venus Surface Observed by the Galileo Near-Infrared Mapping Spectrometer. DPS Meeting #36, #39.22.

Haus, R., Goering, H., 1990. Radiative energy balance of the Venus mesosphere. Icarus 84, 62–82.

Head, J.W., Wilson, Lionel, 1986. Volcanic processes and landforms on Venus—theory, predictions, and observations. J. Geophys. Res. 91, 9407–9446.

Hinson, D.P., Jenkins, J.M., 1993. Magellan radio occultations measurements of atmospheric waves on Venus. Icarus 105, 142–161.

Hou, A.Y., Farrell, B.F., 1987. Superrotation induced bu critical-level absorption of gravity waves on Venus: an assessment. J. Atmos. Sci. 44, 1049–1061.

Hunten, D.M., 1995. Venus lightning: pros and cons. Adv. Space Res. 15, 109–112.

Irwin, P.G.J., Dyudina, U., 2002. The retrieval of cloud structure maps in the equatorial region of Jupiter using a principal component analysis of Galileo/NIMS data. Icarus 156, 52–63.

Kamp, L.W., Taylor, F.W., Calcutt, S.B., 1988. Structure of Venus's atmosphere from modelling of night-side infrared spectra. Nature 336, 360–362.

Kelley, M.C., Livingston, R., McCready, M., 1985. Large amplitude thermospheric oscillations induced by earthquakes. Geophys. Res. Lett. 12, 577–580.

Klose, K.B., Wood, J.A., Hashimoto, A., 1992. Mineral equilibria and the high radar reflectivity of Venus mountaintops. J. Geophys. Res. 97, 16353–16369.

Komatsu, G., Baker, V.R., Gulick, V.C., Parker, T.J., 1993. Venusian channels and valleys—distribution and volcanological implications. Icarus 102, 1–25.

Kurucz, 1998. Modeled solar irradiance. Internal report. File available at ⟨http://kurucz.harvard.edu/sun/IRRADIANCE/⟩.

Little, B., Anger, C.D., Ingersoll, A.P., Vasavada, A.R., Senske, D.A., Breneman, H.H., Borucki, W.J., 1999. The Galileo SSI team, Galileo images of lightning on Jupiter. Icarus 14, 306–323.

Lopes-Gautier, R., McEwen, A.S., Smythe, W.B., Geissler, P.E., Kamp, L., Davies, A.G., Spencer, J.R., Keszthelyi, L., Carlson, R., Leader, F.E., Mehlman, R., Soderblom, L., 1999. The Galileo NIMS and SSI teams active volcanism on Io: global distribution and variations in activity. Icarus 140, 243–264.

López-Valverde, M.A., Drossart, P., Carlson, R., Mehlman, R., Rood-Serote, M., 2007. Non-LTE infrared observations at Venus: from NIMS/Galileo to VIRTIS/Venus Express. Planet. Space Sci., this issue, doi:10.1016/j.pss.2007.01.008.

Ma, Q., Tipping, R.H., 1991. A far wing line shape theory and its application to the water continuum absorption in the infrared region. J. Chem. Phys. 95, 6290–6301.

Marcq, E., Bézard, B., Encrenaz, T., Birlan, M., 2005. Latitudinal variations of CO and OCS in the lower atmosphere of Venus from near-infrared nightside spectro-imaging. Icarus, in press.

Marcq, E., Encrenaz, T., Bézard, B., Birlan, M., 2006. Remote sensing of Venus' lower atmosphere from ground-based IR spectroscopy: latitudinal and vertical distribution of minor species. Planet. Space Sci. 54, 1360–1370.

Marov, M.Ya., Shari, V.P., 1997. Optical characteristics of model aerosols in the atmospheres of Mars and Venus. Solar System Res. 31 (4), 255–276.

Meadows, V.S., Crisp, D., 1996. Ground-based near-infrared observations of the Venus nightside: the thermal structure and water abundance near the surface. J. Geophys. Res. 101, 4595–4622.

Moroz, A., 2002. Estimates of visibility of the surface of Venus from descent probes and balloons. Planet. System Sci. 50, 287–297.

Pettengill, G.H., Ford, P.G., Wilt, R.J., 1992. Venus surface radiothermal emission as observed by Magellan. J. Geophys. Res. 97, 13091–13102.

Piccioni, G. P., Drossart, et al., 2006. VIRTIS (Visible and Infrared Imaging Spectrometer) for Venus Express, ESA-SP 1291.

Pollack, J.B., Strecker, D.W., Witterborn, F.C., Erickson, E., Baldwin, B.J., 1978. Properties of the clouds of Venus as inferred from airborne observations of its near-infrared reflectivity spectrum. Icarus 34, 28–45.

Pollack, J.B., et al., 1993. Near infrared light from Venus' nightside; a spectroscopic analysis. Icarus 103, 1–42.

Price, M.H., Watson, G., Suppe, J., Brankman, J., 1996. Dating volcanism and rifting on Venus using impact crater densities. J. Geophys. Res. 101, 4657–4672.

Revercomb, H.E., Sromovsky, L.A., Suomi, V.E., Boerse, R.W., 1985. Net thermal radiation in the atmosphere of Venus. Icarus 61, 521–538.

Robinson, C.A., Thornhill, G.G., Parfitt, E.A., 1995. Large-scale volcanic activity at Maat Mons: can this explain fluctuations in atmospheric chemistry observed by Pioneer Venus? J. Geophys. Res. 100, 11755–11763.

Rogers, N., Hawkesworth, C., 2000. Composition of magmas. In: Sigurdsson, H., et al. (Eds.), Encyclopedia of Volcanoes. Academic, San Diego, CA, pp. 115–131.

Roldan, C., Lopez-Valverde, M.A., Lopez-Puertas, M., Edwards, D.P., 2000. Non-LTE infrared emissions of CO_2 in the atmosphere of Venus. Icarus 147, 11–25.

Roos, M., Drossart, P., Encrenaz, Th., Lellouch, E., Bézard, B., Carlson, R.W., Baines, K.H., Kamp, L.W., Taylor, F.W., Collard, A.D., Calcutt, S.B., Pollack, J.B., Grinspoon, D.H., 1993. The upper clouds of Venus: determination of the scale height from NIMS/Galileo infrared data. Planet. Space Sci. 41, 505–514.

Roos-Serote, M., Drossart, P., Encrenaz, Th., Lellouch, E., Carlson, R.W., Baines, K.H., Taylor, F.W., Calcutt, S.B., 1995. The thermal structure and dynamics of the atmosphere of Venus between 70 and 90 km from the Galileo-NIMS spectra. Icarus 114, 300–309.

Rossow, W.B., 1983. A general circulation model of a Venus-like atmosphere. J. Atmos. Sci. 40, 273–301.

Rossow, W.B., Williams, G.P., 1979. Large-scale motion in the Venus stratosphere. J. Atmos. Sci. 36, 377–389.

Rossow, W.B., et al., 1980. Cloud morphology and motions from Pioneer Venus images. J. Geophys. Res. 85 (A13), 8107–8128.

Schofield, J.T., Diner, D.J., 1983. Rotation of Venus's polar dipole. Nature 305, 116–119.

Schofield, J.T., Taylor, F.W., 1983. Measurements of the mean solar-fixed temperature and cloud structure of the middle atmosphere of Venus. Q. J. R. Meteor. Soc. 109, 57–80.

Schubert, G., Young, R.E., 1970. The 4-day Venus circulation driven by periodic thermal forcing. J. Atmos. Sci. 27, 523–528.

Seidelmann, P.K., Abalakin, V.K., Bursa, M., Davies, M.E., Bergh, C.d., Lieske, J.H., Oberst, J., Simon, J.L., Standish, E.M., Stooke, P., Thomas, P.C., 2002. Report of the IAU/IAG Working Group on Cartographic Coordinates and Rotational Elements of the Planets and Satellites: 2000. Celestial Mech. Dynam. Astron. 82, 83–111.

Seiff, A., Schofield, T.J., Kliore, A.J., Taylor, F.W., Limaye, S.S., Revercomb, H.E., Sromovsky, L.A., Kerzhanovich, V.V., Moroz, V.I., Marov, M.Y., 1983. Models of the structure of the atmosphere of Venus from the surface to 100 kilometers altitude. Adv. Space Res. 5, 3–58.

Seiff, A., Schofield, J.T., Kliore, A.J., Taylor, F.W., Limaye, S.S., 1985. Models of the structure of the atmosphere of Venus from the surface to 100 km altitude. Adv. Space Res. 5 (11), 3–58.

Seiff, A., et al., 1992. The evidences of waves in the atmospheres of Venus and Mars. In: Venus and Mars: Atmospheres, Ionospheres and Solar wind Interactions, AGU Geophysical Monograph Series 66, Proceedings of the Chapman Conference, Balatonfured, Hungary, Washington, DC, pp. 73–89.

Slanger, T., Wolven, B. C., 2002. Airglow processes in planetary atmosphere. In: Atmospheres in the Solar System, AGU Geophysical Monograph Series 130, Proceedings of the Chapman Conference, Balatonfured, Hungary, Washington, DC, pp. 77–93.

Solomon, et al., 1992. Venus tectonics: an overview of Magellan observations. J. Geophys. Res. 97, 13199–13256.

Strom, R.G., Schaber, G.G., Dawson, D.D., 1994. The global resurfacing of Venus. J. Geophys. Res. 99, 10899–10926.

Svedhem, H., Titov, D.V., McCoy, D., Lebreton, J.-P., Barabash, S., Bertaux, J.-L., Drossart, P., Formisano, V., Häusler, B., Korablev, O., Markiewicz, W.J., Nevejans, D., Pätzold, M., Piccioni, G., Zhang, T.L., Taylor, F.W., Lellouch, E., Koschny, D., Witasse, O., Warhaut, M., Accomazzo, A., Rodriguez-Canabal, J., Fabrega, J., Schirmann, T., Clochet, A., Coradini, M., 2007. Venus Express—The first European mission to Venus. Planet. Space Sci., 2007, this issue, doi:10.1016/j.pss.2007.01.013.

Taylor, F.W., 1990. The Venusian polar dipole. In: Schaeffer, K., Spankuch, D. (Eds.), Middle Atmosphere of Venus, Veroffentlichungen des Forchungsberichs Geo- und Kosmoswischenschaften, vol. 18. Academie-Verlag, Berlin, pp. 93–97.

Taylor, F.W., Beer, R., Chahine, M.T., Diner, D.J., Elson, L.S., Haskins, R.D., McCleese, D.J., Martonchik, J.V., Reichley, P.E., Bradley, S.P., Delderfield, J., Schofield, J.T., Farmer, C.B., Froidevaux, L., Leung, J., Coffey, M.T., Gille, J.C., 1980. Structure and meteorology of the middle atmosphere of Venus: infrared remote sounding from the Pioneer Orbiter. J. Geophys. Res. 85, 7963–8006.

Taylor, F.W., et al., 1983. The thermal balance of the middle and upper atmosphere of Venus. In: Hunten, D.M., Colin, L., Donahue, T.M., Moroz, V.I. (Eds.), Venus. University of Arizona Press, Tucson, pp. 650–680.

Taylor, F.W., Crisp, D., Bézard, B., 1997. Near-infrared sounding of the lower atmosphere of Venus. In: Bougher, S.W., Hunten, D.M., Phillips, R.J. (Eds.), Venus II Geology, Geophysics, Atmosphere and Solar Wind Environment. University of Arizona Press, Tucson, AZ, pp. 325–351.

Titov, D.V., Svedhem, H., Koschny, D., Hoofs, R., Barabash, S., Bertaux, J.-L., Drossart, P., Formisano, V., Häusler, B., Korablev, O., Markiewicz, W.J., Nevejans, D., Pätzold, M., Piccioni, G., Zhang, T.L., Merritt, D., Witasse, O., Zender, J., Accomazzo, A., Sweeney,

M., Trillard, D., Janvier, M., Clochet, A., 2006. Venus Express science planning. Planet. Space Sci. 54, 1279–1297.

Toigo, A., Gierasch, P.J., Smith, M.D., 1994. High resolution cloud feature tracking on Venus by Galileo. Icarus 109, 318–336.

Tonkov, M.V., Filippov, N.N., Bertsev, V.V., Bouanich, J.P., Van-Thanh, N., Brodbeck, C., Hartmann, J.M., Boulet, C., Thibault, F., Le Doucen, R., 1996. Measurements and empirical modelling of pure CO_2 absorption in the 2.3-µm region at room temperature: far wings, allowed and collision-induced bands. Appl. Opt. 35, 4863–4870.

Tvorogov, S.D., Rodimova, O.B., 1995. Spectral line shape, I: kinetic equation for arbitrary frequency detunings. J. Chem. Phys. 102, 8736–8745.

Wattson, R.B., Rothman, L.S., 1986. Determination of vibrational energy levels and parallel band intensities of $^{12}C^{16}O_2$ by direct numerical diagonalization. J. Mol. Spectrosc. 119 (1), 83–100.

Wood, J.A., 1997. Rock weathering on the surface of Venus. In: Bougher, S.W., Hunten, D.M., Phillips, R.J. (Eds.), Venus II. Arizona University Press, Tucson, AZ.

Zimbelman, J.R., 1998. Emplacement of long lava flows on planetary surfaces. J. Geophys. Res. 103, 27503–27516.